Citation information: DOI 10.1109/TIE.2018.2856186, IEEE

Voltage Control of a Standalone Cascaded Doubly Fed Induction Generator

Maria El Achkar, Rita Mbayed, Georges Salloum, *Senior Member, IEEE*, Nicolas Patin, *Senior Member, IEEE*, and Eric Monmasson, *Senior Member, IEEE*

***Abstract*—This paper studies the cascaded doubly fed induction machine, operating as a brushless variable speed constant frequency generator supplying an isolated load. In isolated electric supply, the amplitude and frequency of the output voltage of the generator should be stabilized during the speed and/or load changing. Despite the complexity of the generator model, a simple indirect field oriented vector control is elaborated to meet the output voltage requirements. Experimental results validate the proposed control approach. The study is extended to reveal the behavior of the controlled system under unbalanced load.**

***Index Terms*—Brushless, cascaded doubly fed induction machine, standalone application, variable speed constant frequency, vector control.**

NOMENCLATURE

R_s, R_r	Stator, rotor resistance
L_s, L_r	Stator, rotor cyclic inductance
M_{sr}	Stator to rotor mutual inductance
ω_s, ω_r	Stator, rotor angular frequency
θ_m	Rotor mechanical angular position
Ω	Rotor mechanical speed
$\underline{i}_s, \underline{i}_r$	Stator, rotor current vector
$\underline{v}_s, \underline{v}_r$	Stator, rotor voltage vector
$\underline{\phi}_s, \underline{\phi}_r$	Stator, rotor flux vector
σ_p	Coefficient of dispersion
p_1, p_2	Number of pole pairs of DFIM1, DFIM2
g_c	CDFIM slip ratio
ξ_{s2}	Electrical Park frame angle
$\underline{x}$	Phasor quantity
$\lvert\underline{x}\rvert$	Magnitude of the alternating quantity x
$\tilde{x}$	Estimated quantity
X_d, X_q	d-axis, q-axis components in Park reference frame
dq_2	Stator flux oriented synchronous frame

Subscripts

$1, 2$	Control machine DFIM1, Power machine DFIM2
ref	Reference value
s, r	Stator, rotor

Manuscript received September 28, 2017; revised December 30, 2017 and March 03, 2018 and April 28, 2018 and June 09, 2018; accepted June 27, 2018.

M. El Achkar, R. Mbayed G. Salloum are with "Commande Energies Renouvelables et Génies Electriques" (CERGE), Lebanese University Faculty of Engineering, Roumieh, Lebanon(e-mail: maria.elachkar@gmail.com, rmbayed@ul.edu.lb, georges.salloum@ul.edu.lb).

N. Patin is with "Laboratoire d'Electromecanique" (LEC), University of Technology of Compiègne, Compiègne 60205, France (e-mail: nicolas.patin@utc.fr).

E. Monmasson is with "Systèmes et Applications des Technologies de l'Information et de l'Energie" Laboratory (SATIE), University of Cergy-Pontoise, 95300 Cergy-Pontoise, France (e-mail: eric.monmasson@u-cergy.fr).

I. INTRODUCTION

Due to the recent interest in renewable energy systems and embedded applications and the advance in power electronics, the development and control of variable speed constant frequency generators have become a very important research topic. The brushless doubly fed induction machines are receiving renewed attention as sources of constant voltage, constant frequency power from variable speed prime movers, especially in applications where high level of reliability and long time maintenance periodicity are required such as high power wind generation, hydro-power systems, aircraft and marine shaft electrical power generation. Indeed, this doubly fed generator can be directly connected to the grid/isolated load and provide constant voltage constant frequency electric power thanks to the regulation of the control machine windings. Besides, in grid-connected operation, the generator can supply reactive current and achieve independent control of the output active and reactive powers. The generator is driven by a low power converter, fixed by the range of the operating speed. The absence of brushes offers robustness, high reliability and low maintenance requirements, which are fundamental in the above-mentioned applications [1], [2]. The brushless doubly fed induction machine is regarded as a potential alternative to the popular Doubly Fed Induction Machine (DFIM). It shows commercial promises for either grid-connected or standalone operation [1], [3], [4].

The Cascaded Doubly Fed Induction Machine (CDFIM) is the basic concept of a doubly fed brushless machine. It is simply formed by two wound rotor induction machines affixed to the same shaft with their rotor windings connected. This early version has then evolved from a structure based on two separated machines to a single compact electric machine. In 1970, Broadway proposed to merge the two sets of stator windings by a dual-tapped stator windings wound into a common stator core [5]. The stator windings must differ in the number of pole pairs to avoid direct coupling between the windings. Besides, the common rotor is specially designed to induce a cross-coupling effect between the two stators, with the pole number being half the sum of the stator poles.

Citation information: DOI 10.1109/TIE.2018.2856186, IEEE

The machine performances and power density improve as this mutual coupling is improved. The rotor configuration can be divided into special nested cage type and reluctance type, introducing two descendants of the CDFIM: the Brushless Doubly Fed Induction Machine (BDFIM) and the Brushless Doubly Fed Reluctance Machine (BDFRM) respectively. It is shown that the rotor design and the selection of pole number combination are keys to the power density, and efficiency of the machine [6]. As pointed, several design alternatives of the CDFIM exist; however this work is limited to the conceptual case of two cascaded DFIMs. This representation being sufficient when it comes to control design.

The majority of research interests related to the CDFIG are concerned by the grid-connected operation. Various models and control methods are elaborated with attention being paid towards their application in wind power generation systems. The maximum power point tracking and the independent regulation of active and reactive powers have been intensively studied [7]–[9]. The active-reactive power operating margins of the generator were also analyzed in [10]. Recently, the transient behavior of the grid-connected generator is the main research topic. Voltage regulation and ride-through capability of the wind turbine during grid faults [11], [12], and compensation of unbalanced network [4], [13] are being investigated.

Nevertheless, with its brushless structure, reduced size converters and constant amplitude constant frequency output voltage, the CDFIG is suitable for many industrial autonomous applications where variable speed constant frequency operation is required. In this sense, in order to assess the full potential and capability of this generator, new voltage control methods of the standalone CDFIG and similar topologies, in particular BDFIG, are being investigated in recent years. A scalar control strategy was proposed in [14]. The approach, based on steady-state model and Fuzzy PID, is interesting but unfortunately the response does not comply with the dynamic requirements and the control was only tested by simulation. In [1], a modeling methodology of the autonomous CDFIG based on dynamical equivalent circuits is suggested. The global equivalent model of the CDFIG is represented by a complex conjugate transformer; where the two DFIMs are described in their respective stator reference frames. Then, this model is used for the design of the machine controller, based on the model inversion principle. The problem in the proposed method is that the control is dependent of the machine parameters and the machine model is described in multiple reference frames giving way to a multiple-frequency control approach. A voltage and current double closed-loop control strategy of a "double-sine" wound BDFIM is elaborated in [15]. The voltage amplitude regulation is deduced from the BDFIM steady-state per-phase equivalent circuit. The method is based on control winding current decoupling using control winding field orientation. Yet, by examining the simulation/experimental results, it seems that the control approach did not yield to high dynamic performances: response is relatively slow with a significant overshoot in the voltage amplitude at load variation. In addition, as pointed by the paper authors, voltage fluctuation in the power winding can be observed for a certain speed range due to the presence of a pair of symmetrical harmonic waves, and a compensation strategy with harmonic injection is thus carried out at a specific speed range to reduce the inter-harmonic contents. A Decoupling Network (DN) design for the d-q vector model of a BDFIG was recently proposed in [16]. The method tends to avoid Feed-Forward (FF) compensation terms that require extra sensors, and have highly parameter dependency. Although, the simulation/experimental results are satisfactory, the main concern in the suggested method is that the DN is in series with the BDFIG and the load. Consequently, the obtained control plant to be regulated becomes load and speed dependent, which influences the design of the controller and the response of the system for a wide range of load and speed variation. In addition, the presented approach requires the implementation of DN terms in the control loop to overcome the coupling effect, thereby amplifies the computational time and complexity order of the algorithm for real time implementation. These DN terms are function of the rotor speed and parameters of the machine, which increases the sensitivity of the controller to the parameter deviation and speed variation.

In this paper, a new vector control of the standalone CDFIG is presented. The control scheme is elaborated based on the vector model of the generator in the unified synchronous reference frame, and aims to adjust the amplitude and frequency of the output voltage irrespective of load and speed variation. An indirect stator field orientation is proposed, in which the stator flux angle is not derived from voltage measurement and is thus shielded from noise and possible harmonic distortion on the stator voltage. The field orientation and the terminal voltage are separately controlled. The voltage magnitude is adjusted by action on the rotor current d-component. The q-axis component is used to force the reference frame orientation. The main contribution of this work, is that the control plant to be regulated is composed of first order transfer functions, which facilitates the controller design. The controller is totally independent of the load; therefore it remains applicable for any load and shall not be revised. In addition, no FF terms nor DN algorithm are required in this method. The controller is able to provide good decoupling feature, while achieving good dynamic and permanent state behavior. Consequently, the real time implementation is simplified and the robustness of the controller to parametric uncertainties of the system would be no doubt improved. The paper presents in addition an experimental validation of the proposed control strategy. Experiments considering load-disturbance are further investigated in this work.

The rest of the paper is organized as follows: the dynamic behavior of the CDFIG is elaborated in section II. The control strategy of the standalone generator is detailed in section III. In section IV, the control approach is validated by simulations in a first place. A comparison with the conventional FF method is presented. The results are then compared with those obtained experimentally. The system is tested with reference voltage, load and rotational speed variations using a laboratory scale CDFIM. The performance of the controlled system is further tested under parameter deviation and unbalanced load. The obtained results are satisfactory.

Citation information: DOI 10.1109/TIE.2018.2856186, IEEE

II. Modeling of the CDFIG

A. Configuration of the standalone generator

The CDFIG is composed of two wound rotor induction machines connected in cascade (Fig.1). The two rotors are mechanically and electrically coupled eliminating the need of brushes [1]. The two machines can theoretically have any pole pair combination (p_1, p_2) with the rotors electrically connected in positive or in negative phase sequence. Nevertheless, the power flow analysis established in [1] has shown that the direct interconnection configuration must be avoided. In fact, for $p_1 = p_2$ there is no global electromechanical conversion thus the CDFIM performs as a static transformer, and for $p_1 \neq p_2$ the signs of the two mechanical powers are different thus the two DFIMs operate in a combined motor/generator mode. The only satisfying performances for generating systems are achieved by an inverse coupling sequence since the total mechanical power is provided by both DFIMs, proportionally to their respective number of pole pairs. This allows the torques to combine in the additive manner.

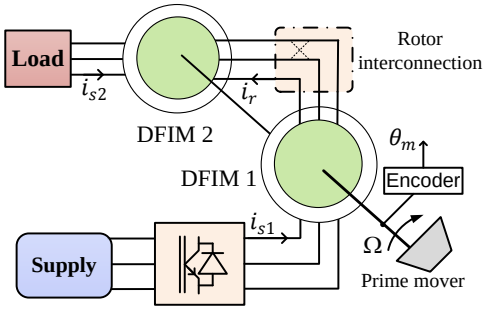

Fig. 1. Configuration of the standalone CDFIG.

The major interest of a CDFIG is the operation in synchronous mode [17]. The machine is able to operate stably as a brushless variable speed generator over a wide speed range with controllable dynamic response [18]. The synchronous operation occurs when the rotor currents, induced by both machines, evolve with the same frequency [19]. This way, the Power machine (DFIM2) windings can be controlled through the rotors from the Control machine (DFIM1) stator in a brushless manner. Under this operating mode, the frequency behavior of the CDFIG is expressed by (1).

$$\omega_{s1} = (p_1 + p_2)\Omega - \omega_{s2} \tag{1}$$

Therefore, the CDFIG can provide a constant output frequency ω_{s2} by regulating the Control machine stator frequency ω_{s1} irrespective of rotor speed variation.

B. Vector model

The main difficulty when working with the CDFIM is its inherent complexity, and the existence of multiple reference frames. The major issue is to synthesize an efficient global control method for these two connected machines. A space phasor model of the CDFIM in a common reference frame with a given pole pair distribution related to one of the two machines is proposed and verified experimentally in [20]. In this unified coordinate, the dynamic model of the CDFIM is independent of the rotor angle position and analogous to the DFIM model. This representation is appropriate for the elaboration of new control strategies despite the complex structure of the system. The vector model of the CDFIM in the unified Power machine synchronous frame (dq_2) is given by (2) to (7) [21]. 1 and 2 subscripts refer to DFIM1 and DFIM2 quantities respectively. In what follows, phasors are denoted by underlined lower case characters and the phasor components by upper case characters.

$$\underline{v}_{s2} = R_{s2}\underline{i}_{s2} + \frac{d}{dt}\underline{\phi}_{s2} + j\omega_{s2}\underline{\phi}_{s2} \tag{2}$$

$$\underline{v}_{s1} = R_{s1}\underline{i}_{s1} + \frac{d}{dt}\underline{\phi}_{s1} + j\left(\omega_{s2} - (p_1 + p_2)\Omega\right)\underline{\phi}_{s1} \tag{3}$$

$$0 = R_r\underline{i}_r + \frac{d}{dt}\underline{\phi}_r + j\left(\omega_{s2} - p_2\Omega\right)\underline{\phi}_r \tag{4}$$

$$\underline{\phi}_{s2} = L_{s2}\underline{i}_{s2} + M_{sr2}\underline{i}_r \tag{5}$$

$$\underline{\phi}_{s1} = L_{s1}\underline{i}_{s1} - M_{sr1}\underline{i}_r \tag{6}$$

$$\underline{\phi}_r = L_r\underline{i}_r + M_{sr2}\underline{i}_{s2} - M_{sr1}\underline{i}_{s1} \tag{7}$$

where Φ_r is a fictitious quantity representing the rotor circuit loop flux linkage, and:

$$L_r = L_{r1} + L_{r2}; \qquad R_r = R_{r1} + R_{r2} \tag{8}$$

III. Voltage Control of the Standalone Generator

In the targeted standalone application, the CDFIG is driven at a variable speed and supplies an isolated three-phase load. The controller must provide constant frequency and amplitude for the terminal voltage in spite of load and/or speed variation. Unlike grid-connected systems, the output stator voltage in standalone applications is no longer established by the grid and can be regulated by action on the rotor current. An indirect stator field oriented decoupled vector control is adopted to adjust the output voltage $\underline{v}_{s2}$ of the CDFIG. The approach is based on cascaded loops with two regulation paths, devoted to control the rotor current d-axis and q-axis components distinctly. The voltage magnitude is controlled by action on one of the rotor current components. The other component is used to force the reference frame orientation.

If stator field orientation is considered with the d-axis aligned along the stator flux vector $\underline{\phi}_{s2}$, the following relations are deduced:

$$\Phi_{s2q} = 0; \qquad \Phi_{s2d} = \left|\underline{\phi}_{s2}\right| \tag{9}$$

Introducing (9) in (5) and decomposing into d-q components yields to:

$$I_{s2q} = -\frac{M_{sr2}}{L_{s2}}I_{rq} \tag{10}$$

$$I_{s2d} = \frac{\Phi_{s2d}}{L_{s2}} - \frac{M_{sr2}}{L_{s2}}I_{rd} \tag{11}$$

Referring to (2), (9), (10) and (11), the dynamic behavior of the stator flux is expressed as:

$$\frac{1}{M_{sr2}}\Phi_{s2d} + \frac{L_{s2}}{R_{s2}M_{sr2}}\frac{d}{dt}\Phi_{s2d} = \frac{L_{s2}}{R_{s2}M_{sr2}}V_{s2d} + I_{rd} \tag{12}$$

$$V_{s2q} = R_{s2}I_{s2q} + \omega_{s2}\Phi_{s2d} \tag{13}$$

Citation information: DOI 10.1109/TIE.2018.2856186, IEEE

At steady state, the grid voltage magnitude should be maintained constant. Neglecting the resistive voltage drop with regard to the back EMF $\omega_{s2}\Phi_{s2d}$, the following relations are obtained:

$$V_{s2d} \simeq 0 \tag{14}$$

$$V_{s2q} \simeq \omega_{s2}\Phi_{s2d} \simeq |\underline{v}_{s2}| \tag{15}$$

It can be noticed from (12) and (15) that I_{rd} and the voltage amplitude $|\underline{v}_{s2}|$ are linked by a first order transfer function. The voltage d-axis component V_{s2d} is considered as a disturbance. Since the influence of V_{s2d} is negligible, the voltage magnitude, can be directly controlled by adjusting the rotor current d-component. In this context, the rotor current q-component forms a degree of freedom, it is thus manipulated to force the vector orientation of (dq_2) along the stator flux. The required I_{rq} set point is derived from the condition of $\Phi_{s2q} = 0$ as:

$$I_{rq,ref} = -\frac{L_{s2}}{M_{sr2}} I_{s2q} \tag{16}$$

Notice that I_{rq} must track its reference under the action of a fast control loop (compared to the voltage control loop) to reach an effective reference orientation. This approach may be denoted: "indirect stator flux orientation vector control". The orientation condition means that the frame angle (the Park angle) ξ_{s2} can be derived from a simple integral of the output frequency demand $\omega_{s2,ref}$ as shown in (17). It does not have to be computed from stator voltage measurement or stator flux estimated from the machine model, since the orientation is forced by the condition (16).

$$\xi_{s2} = \int \omega_{s2,ref} dt \tag{17}$$

Therefore the output voltage measurement or the Power machine stator flux do not interfere in the orientation scheme. Consequently, the orientation is more stable, robust to load changes and devoid of measurement noise and possible harmonic distortion on the stator voltage; particularly in weak networks with disturbances or unsymmetrical conditions. These harmonics would be intensified if the orientation angle was calculated from voltage measurement.

Referring to (4) and (7), relation (18) is established between the machine currents as:

$$(R_r + j\omega_r L_r)\,\underline{i}_r + L_r \frac{d}{dt}\underline{i}_r + j\omega_r M_{sr2}\underline{i}_{s2} + M_{sr2}\frac{d}{dt}\underline{i}_{s2} - j\omega_r M_{sr1}\underline{i}_{s1} - M_{sr1}\frac{d}{dt}\underline{i}_{s1} = 0 \tag{18}$$

where $\omega_r = \omega_{s2} - p_2\Omega$ is the rotor angular frequency. Substituting the quantity of $\frac{d}{dt}\underline{i}_{s2}$ using (5) gives:

$$(R_r + j\omega_r L_r)\,\underline{i}_r + \sigma_p L_r \frac{d}{dt}\underline{i}_r + j\omega_r M_{sr2}\underline{i}_{s2} + \frac{M_{sr2}}{L_{s2}}\frac{d}{dt}\underline{\phi}_{s2} - j\omega_r M_{sr1}\underline{i}_{s1} = M_{sr1}\frac{d}{dt}\underline{i}_{s1} \tag{19}$$

with σ_p being the coefficient of dispersion given by (20).

$$\sigma_p = 1 - \frac{M_{sr2}^2}{L_{s2}L_r} \tag{20}$$

On the other side, the Control machine stator current and voltage $\underline{i}_{s1}$ and $\underline{v}_{s1}$ respectively, and the rotor current $\underline{i}_r$ are related by (21) with $g_c\omega_{s2} = \omega_{s2} - (p_1 + p_2)\,\Omega$.

$$\underline{v}_{s1} = R_{s1}\underline{i}_{s1} + L_{s1}\frac{d}{dt}\underline{i}_{s1} - M_{sr1}\frac{d}{dt}\underline{i}_r + jg_c\omega_{s2}L_{s1}\underline{i}_{s1} - jg_c\omega_{s2}M_{sr1}\underline{i}_r \tag{21}$$

Introducing the expression of $\frac{d}{dt}\underline{i}_{s1}$ from (19) into (21) yields to:

$$\underline{v}_{s1} = \frac{L_{s1}R_r}{M_{sr1}}\underline{i}_r + \left(\frac{\sigma_p L_r L_{s1}}{M_{sr1}} - M_{sr1}\right)\frac{d}{dt}\underline{i}_r + R_{s1}\underline{i}_{s1} + \frac{L_{s1}M_{sr2}}{L_{s2}M_{sr1}}\frac{d}{dt}\underline{\phi}_{s2} - jp_1\Omega L_{s1}\underline{i}_{s1} + j\omega_r\frac{L_{s1}M_{sr2}}{M_{sr1}}\underline{i}_{s2} + j\left(\omega_r\frac{L_r L_{s1}}{M_{sr1}} - g_c\omega_{s2}M_{sr1}\right)\underline{i}_r \tag{22}$$

Then, decomposing into d-q components, the following expressions are obtained:

$$\frac{L_{s1}R_r}{M_{sr1}}I_{rd} + \left(\frac{\sigma_p L_r L_{s1}}{M_{sr1}} - M_{sr1}\right)\frac{d}{dt}I_{rd} = V_{s1d} - a_d \tag{23}$$

$$\frac{L_{s1}R_r}{M_{sr1}}I_{rq} + \left(\frac{\sigma_p L_r L_{s1}}{M_{sr1}} - M_{sr1}\right)\frac{d}{dt}I_{rq} = V_{s1q} - a_q \tag{24}$$

As it can be noticed, $\underline{v}_{s1}$ and $\underline{i}_r$ d-q components are linked by a first order linear transfer function. The factors a_d and a_q, given by the following relations, define the d-q disturbances composed of a cross coupling perturbation and back EMF related to DFIM2 stator flux.

$$a_d = R_{s1}I_{s1d} + \frac{L_{s1}M_{sr2}}{L_{s2}M_{sr1}}\frac{d}{dt}\Phi_{s2d} + p_1\Omega L_{s1}I_{s1q} - \left(\omega_r\frac{L_r L_{s1}}{M_{sr1}} - g_c\omega_{s2}M_{sr1}\right)I_{rq} - \omega_r\frac{L_{s1}M_{sr2}}{M_{sr1}}I_{s2q} \tag{25}$$

$$a_q = R_{s1}I_{s1q} - p_1\Omega L_{s1}I_{s1d} + \omega_r\frac{L_{s1}M_{sr2}}{M_{sr1}}I_{s2d} + \left(\omega_r\frac{L_r L_{s1}}{M_{sr1}} - g_c\omega_{s2}M_{sr1}\right)I_{rd} \tag{26}$$

Consequently the rotor current components I_{rd} and I_{rq} can be adjusted by action on the Control machine stator voltage V_{s1d} and V_{s1q} respectively.

On the basis of previous relations, the open-loop transfer function of the standalone CDFIG in the predefined field oriented synchronous (dq_2) frame is deduced. The plant to be regulated is thus illustrated in Fig.2. As it can be observed,

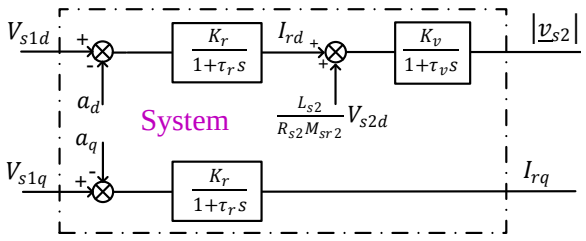

Fig. 2. Open loop transfer function of the standalone generator

a decoupled vector control of the CDFIG can be achieved with the stator flux orientation. The output voltage is regulated

Citation information: DOI 10.1109/TIE.2018.2856186, IEEE

through two hierarchical loops using PI controllers (refer to Fig.5). An outer loop to adjust the voltage amplitude and an inner faster loop to control the rotor current and force the indirect field orientation. The output of the voltage control loop forms the rotor current demand $I_{rd,ref}$. The voltage references $V_{s1d,ref}, V_{s1q,ref}$ are provided by the rotor current controllers. Compensation terms $\tilde{a}_d$, $\tilde{a}_q$, based on (25) and (26), are commonly added by a feed-forward action to the output of the PI controllers to provide linear transfer function and overcome the coupling perturbations. However, the feed-forward method requires extra sensors to measure the control current, involves additional dq frame transformation of the sensed variable and it heavily depends on the parameter accuracy and the quality of the measured quantities. Moreover, some feed-forward terms are physically unrealizable, and thus have to be simplified for digital implementation. All these factors degrade the decoupling performances.

To tackle this problem, these compensation terms are discarded in the proposed control strategy. The PI controller is able to provide effective decoupling feature and suppress the d-q perturbation effects while achieving good dynamic response. Consequently, no extra sensors are required, the real time implementation of the control algorithm is simplified, the execution time is reduced, and the robustness of the controller to parametric deviation would be no doubt improved.

Hereinafter, the study is detailed for a laboratory scale CDFIG. The parameters are given in Table I. The proposed control scheme is illustrated in Fig.3. $n_1(s)$ and $n_2(s)$ denote the measurement noise. A delay transfer function $D(s)$ is included to take into account the delay due to the digital computation and the DPWM. For the rotor current control

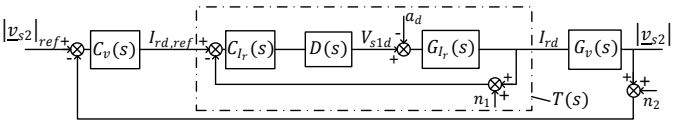

Fig. 3. Block diagram of voltage control loop

loop, the coupling perturbations a_d and a_q are considered as disturbance inputs. They can be transferred to the output side using $w_y(s) = -G_{I_r}(s) * a_d(s)$. Consequently, the following relation can be easily established:

$$I_{rd}(s) = S(s)w_y(s) + T(s)\left(I_{rd,ref}(s) - n_1(s)\right) \qquad (27)$$

where $S(s) = 1/(1 + C_{I_r}.D.G_{I_r})$ is the output sensitivity function. It represents the sensitivity of the output to the disturbances $w_y(s)$ at the output. And $T(s) = (C_{I_r}.D.G_{I_r})/(1+ C_{I_r}.D.G_{I_r})$ is the complementary sensitivity function (also denoted the closed-loop transfer function). It determines the relation between the output and the reference main input as well as the effect of measurement noise on the output signal. These two transfer functions are related by (28).

$$T(s) + S(s) = 1 \qquad (28)$$

The closed-loop transfer function $T(s)$ defines the dynamic behavior of the system. In particular, the response time is inversely proportional to the closed-loop bandwidth. Moreover, relation (27) implies that in order to reject the perturbation effect, it is necessary to have $|S(j\omega)| < 1$ at the frequency range of the disturbance. On the other hand, the measurement noise are attenuated only if $|T(j\omega)| < 1$ [22]. However, relation (28) at first sight makes these requirements contradictory. Therefore, the controller design must achieve a trade-off between the control performances, perturbation rejection and attenuation of measurement errors. Practically, reference signals and disturbances are low frequency signals while noise measurement extends into a much higher frequency range. Thus, an adequate choice of the controller is to make $|S(j\omega)|$ sufficiently attenuated at low frequencies and $|T(j\omega)|$ at high frequencies [22]. A PI controller $C_{I_r}(s) = 7.13(1+\frac{1}{0.0061s})$ is synthesized to achieve a zero steady state error and a settling time of the closed-loop equal to the open-loop settling time. The bode diagram of the two sensitivity functions $S(s)$ and $T(s)$ are shown in Fig. 4. The balance between the two sensitivity functions is highlighted in the figure. As can be seen in Fig. 4, $|S(j\omega)|$ is sufficiently attenuated at low frequency, implying that the coupling effect introduced by the disturbance elements is correctly rejected.

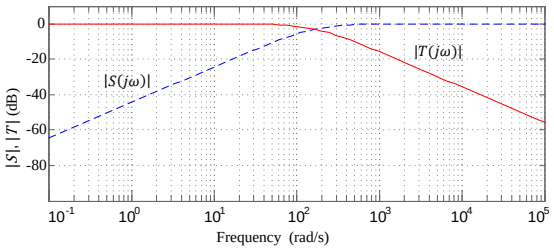

Fig. 4. Characteristics of the sensitivity functions $S(s)$ and $T(s)$

For the outer voltage loop given in Fig.3, a PI controller $C_v(s) = 0.0871(1 + \frac{1}{0.208s})$ is designed to meet a zero steady state error and a settling time of the closed-loop five times smaller than the open-loop settling time.

Since the rotor current is not accessible, a simple open-loop current estimator is proposed hereinafter [1]:

$$\underline{\tilde{\phi}}_{s2} = \int \left(\underline{v}_{s2} - R_{s2}\underline{i}_{s2}\right) dt \qquad (29)$$

$$\underline{\tilde{i}}_r = \frac{1}{M_{sr2}}\left(\underline{\tilde{\phi}}_{s2} - L_{s2}\underline{i}_{s2}\right) \qquad (30)$$

Based on the measured stator voltage and current, the control scheme of the standalone CDFIG is implemented in Fig.5. The Power machine stator quantities are transformed from the original (abc_{s2}) to the predefined rotating (dq_2) frame by performing a Clarke transformation to $(\alpha\beta_{s2})$ followed by a Park transformation with the frame angle ξ_{s2}. At the output of the controller, the voltage references $V_{s1d,ref}, V_{s1q,ref}$ are established in DFIM2 synchronous frame (dq_2). Therefore a transformation (by rotation) back to the DFIM1 three-phase stator frame (abc_{s1}) is required to engender the sinusoidal reference values for the inverter. It is attained using the vector transformation (31) followed by a Clarke transformation, which induces the DFIM2 stator quantities to operate at the

Citation information: DOI 10.1109/TIE.2018.2856186, IEEE

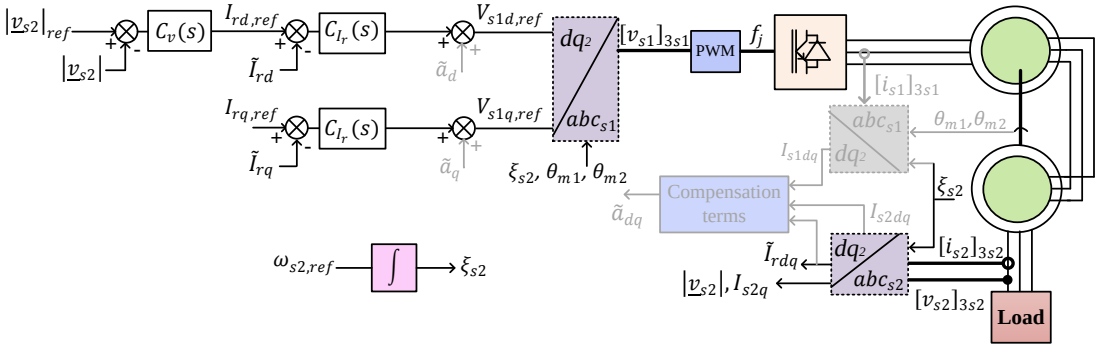

Fig. 5. Control scheme of the standalone CDFIG

demand frequency $\omega_{s2,ref}$ for any shaft speed, during steady state and transient conditions.

$$(\underline{x})_{\alpha\beta_{s1}} = e^{-j(\xi_{s2}-p_1\theta_{m1}-p_2\theta_{m2})}(\underline{\hat{x}})_{dq_2} \tag{31}$$

θ_{m1} and θ_{m2} are the absolute mechanical angular position of each rotor with respect to its corresponding stator, and $\underline{\hat{x}}$ the conjugate of the phasor quantity.

IV. Experimental Verification

A. Experimental setup

Experiments are carried out to test and validate the performances of the proposed control strategy. The laboratory scale bench is illustrated in Fig.6. It comprises two wound rotor induction machines of 2.5 kW each. Their parameters are listed in Table I. Due to facilities, the set is driven by a servo-controlled synchronous motor of 2kW which force us to downgrade the output voltage and power of the CDFIG. The mechanical speed of the prime mover is adjusted by a universal drive UNIDRIVE SP control unit. Notice that the DFIMs are magnetically independent. Their shafts are directly coupled and the rotor windings are interconnected through inverse sequence. The Control machine is supplied with a Pulse Width Modulation (PWM) inverter based on Insulated Gate Bipolar Transistors (IGBT). The IGBT inverter operates at 5 kHz, its control signals are generated by a Xilinx Spartan-3 FPGA. An incremental encoder of 4096 pulses per revolution (ppr) is mounted on the shaft to detect the rotor position. It should be noted that the absolute rotor position is required for the transformation of the machine variables to (dq_2) reference frame. Thus, the initial rotor position of each DFIM is needed to obtain correct alignment.

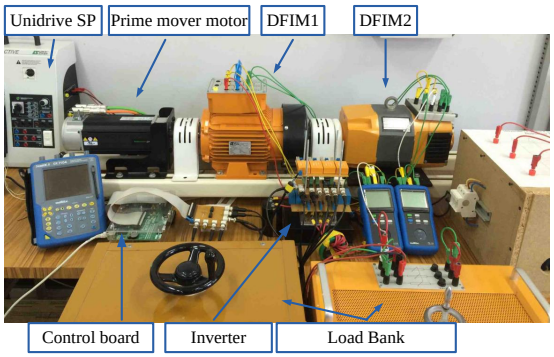

Fig. 6. CDFIM: experimental test bench

TABLE I
PARAMETERS OF THE LABORATORY SCALE MACHINE

Parameters	DFIM1	DFIM2
Rated power active P_{s1n}, P_{s2n} (kW)	2.5	2.5
Rated output voltage V_{s2n} (V)	-	220
Rated stator current I_{s2n} (A)	-	5.5
Number of pole pairs p_1, p_2	2	2
Supply frequency (Hz)	-	50
Stator resistance R_{s1}, R_{s2} (Ω)	4.66	1.29
Rotor resistance R_{r1}, R_{r2} (Ω)	0.92	1.97
Stator cyclic inductance L_{s1}, L_{s2} (mH)	473.28	268.54
Rotor cyclic inductance L_{r1}, L_{r2} (mH)	81.07	138.21
Rotor/stator mutual inductance M_{sr1}, M_{sr2} (mH)	191.43	182.76

B. Simulation and experimental results

Three tests are conducted: control with load variation, with speed variation and with reference voltage variation. For comparison purpose, the controller with FF terms is also designed for simulation.

The first test is done at constant speed ($\Omega = 1.1$p.u.) with load varying from 25% up to 100% of the nominal stator current. The machine stator and the load are star-connected, via a three-wire connection system. The simulation results are collected in Fig.7. The output voltage is properly controlled at constant frequency and magnitude. The voltage amplitude remains equal to its reference despite the load variation. The rotor current responds correctly to the load change. As the connected load increases, a greater rotor current is required to maintain a constant output voltage. Moreover, it is shown that the two control methods (with and without FF) present similar tracking performances of the output voltage and rotor current. A close examination of the transient response reveals comparable behavior in terms of settling time and overshoot.

The experimental measurements are presented in Fig.8. The results comply with those obtained by simulation under the same conditions. The RMS voltage and current waveforms as well as the rotor current d-q step response reveal the good dynamic behavior and decoupling transient response of the controller. It is noted that the steady state rotor current, measured experimentally, is slightly greater (by maximum

Citation information: DOI 10.1109/TIE.2018.2856186, IEEE

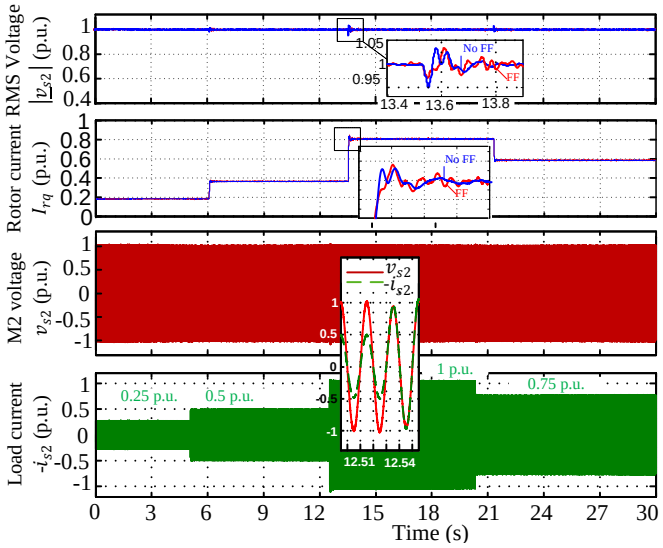

Fig. 7. Simulation results under load variation

8%) than the one obtained by simulation. This is due to the iron losses and saturation that are not taken into consideration in the machine simulation model. The small difference noted between the estimated and the measured rotor current arises from parameter identification error.

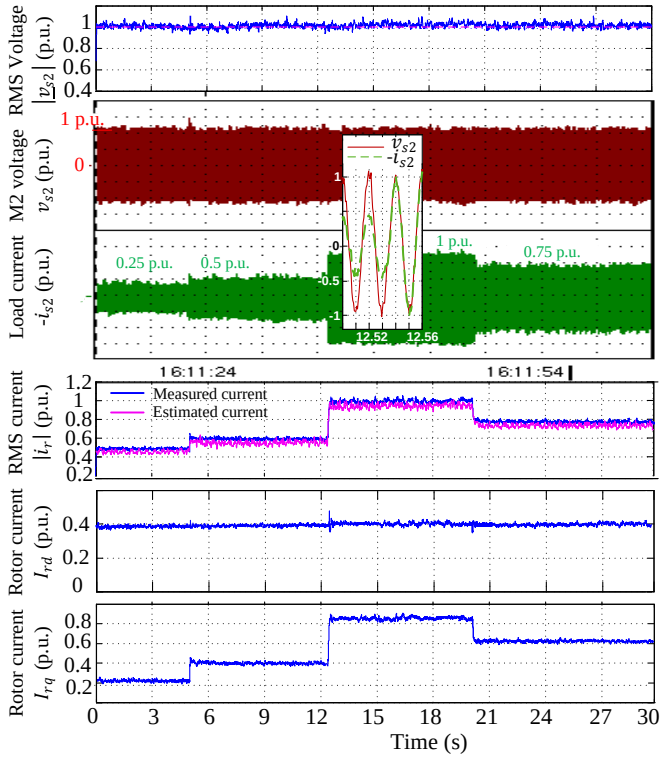

Fig. 8. Experimental results under load variation

The second test is performed at 50% of the nominal stator current. The machine is tested in both subsynchronous and supersynchronous modes. The speed goes from 1.1p.u. down to 0.68p.u. and then increases to 1.23p.u. The response of the CDFIG to speed variation is illustrated in Fig.9. The experimental measurements, under the same speed changes, are given in Fig.10.

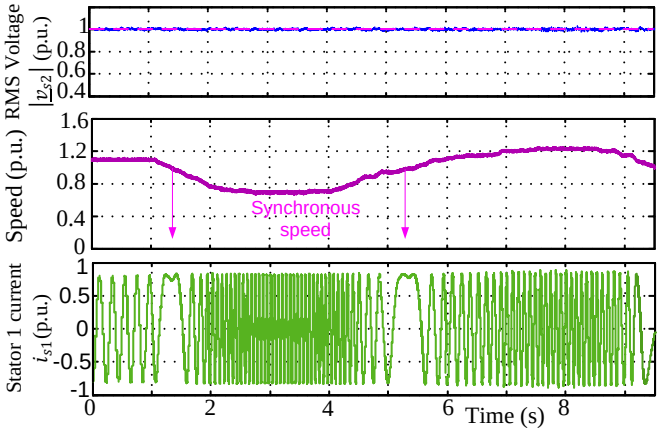

Fig. 9. Simulation results under speed variation

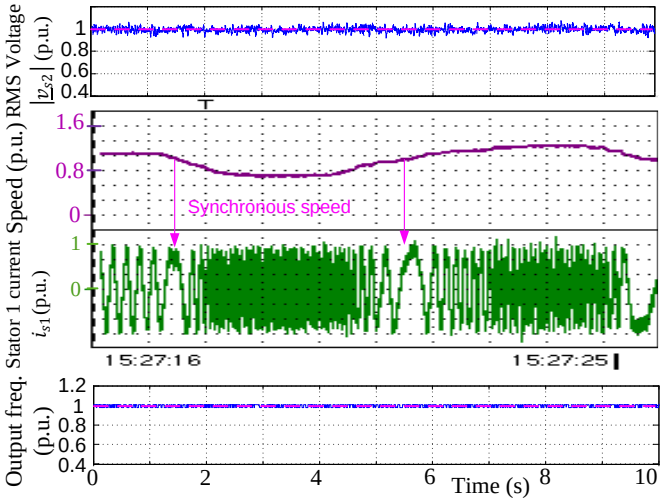

Fig. 10. Experimental results under speed variation

The results show the precise tracking of the voltage amplitude to its reference. The speed disturbance is properly rejected by the controller. The grid frequency is maintained constant in spite of speed variation, thereby variable speed constant frequency operation is achieved. The Control machine stator current reacts correctly, its frequency is adapted to compensate any speed change. The experimental results match those obtained by simulation. The control current attained by simulation is very close to the one measured experimentally. Less than 10% difference is recorded.

The third test is conducted under reference voltage variation. The test is done at 75% of the nominal stator current at constant speed $\Omega = 1.1$p.u. The reference voltage varies between 0.5p.u. and 1.2p.u. The performance of the proposed controller under parameter mismatches is further evaluated in this test. In fact, the control method requires the estimation of the rotor current, which depends on the machine electrical parameters. Yet, these parameters are easy to vary with the generator state especially when the machine runs in saturation. In addition, the identification of the machine parameters might

Citation information: DOI 10.1109/TIE.2018.2856186, IEEE

be not accurate enough. Therefore, the system parameter uncertainties might affect the control behavior. In order to assess the robustness of the proposed approach, the control is tested by simulation with electric parameter variation. The resistances, R_{si} and R_{ri} $i = \{1, 2\}$, are varied by $\pm 50\%$. The inductances, L_{si}, L_{ri}, and M_{sri} vary simultaneously by $\pm 25\%$. The simulation results are given in Fig.11.

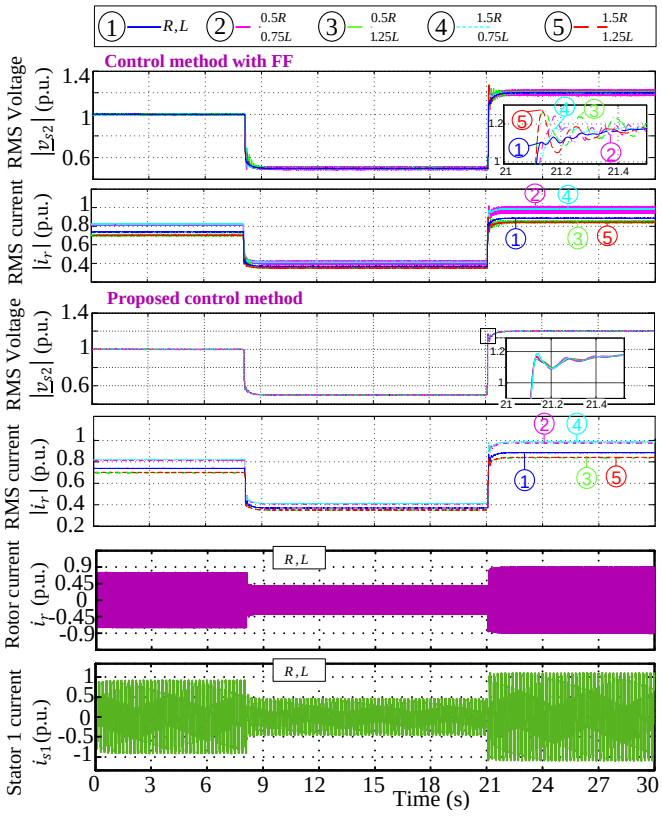

Fig. 11. Simulation results under reference voltage variation and inaccurate machine parameters

As shown, the output voltage keeps a good track of its reference value. The rotor and control currents react correctly to the reference voltage change. The increase of the reference voltage results in an increase of the rotor current and the Control machine stator current. In addition, the results attest that in spite of the parameters deviation the dynamic tracking performances of the proposed controller are satisfactory, the output voltage requirements are met and the system remain stable. The error in the rotor current estimation, due to parameter mismatches, is compensated by the outer voltage control loop. The influence of parameter mismatches on the control performances and system stability can be conveniently confirmed by Bode diagrams in Fig 12. The results prove that even with critical parameter deviation, the cutoff frequency and the phase margin of the controlled system remain nearby their nominal value. This ensures stability and good dynamic performances of the proposed controller. Besides, in the proposed control strategy no FF actions are included, this allows improving the robustness of the controller against parameter variations. Whereas, for the FF method, the transient performance of the system is degraded under parameter variation: overshoot and oscillations are induced in the voltage amplitude and rotor current so the system might become unstable. This is due to the fact that the FF terms are highly dependent of the machine electrical parameters.

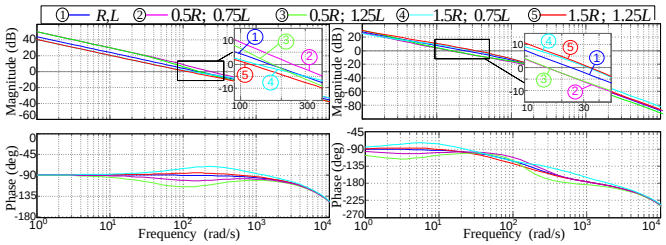

Fig. 12. Bode plots of the compensated open-loop transfer functions: the rotor current $G_{I_r}.C_{I_r}.D$ (left) and the stator voltage $T.G_v.C_v$ (right)

The experimental results under reference voltage variation are given in Fig.13. The results are very close to those obtained by simulation under the same conditions. The small differences in the rotor and Control machine stator current magnitudes arise from iron losses and saturation in the CDFIM in addition to inevitable parameter identification error.

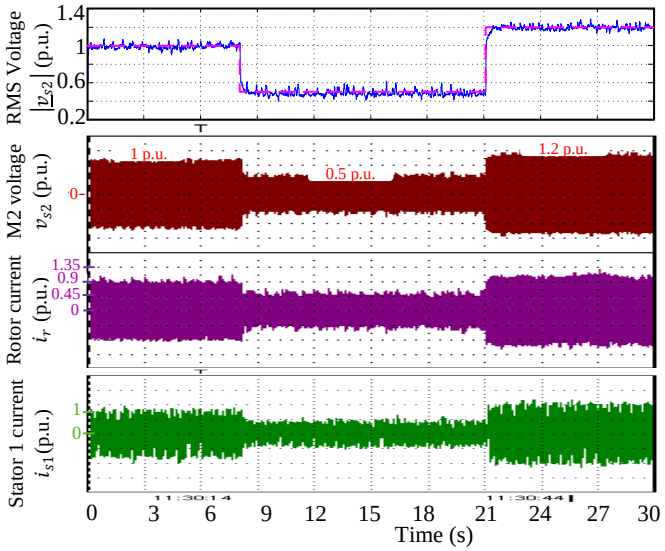

Fig. 13. Experimental results under reference voltage variation

C. Performance under unbalanced load

Previous results consider normal grid conditions. The generator supplies three-phase balanced load. However, in isolated applications, unsymmetrical conditions such as unbalanced loads exist and can have a strong influence on the performances of the generator and the standalone configuration [23]. For this reason, the behavior of the controller under unbalanced operation is worthy to be tested. The connection of unbalanced loads to the stator terminals of the standalone generator induces unbalanced three-phase voltage at the Point of Common Coupling (PCC) due to the unbalanced load current, and give rise to a negative sequence component [23]. Indeed the unbalanced load current causes an unbalanced voltage drop

Citation information: DOI 10.1109/TIE.2018.2856186, IEEE

across the internal stator impedance of the CDFIG, which results in unbalanced stator voltage at the PCC.

In standalone application, the main concern is the regulation of the output voltage in order to preserve the overall dynamic system performances and protect the behavior of other connected loads [23]. The effect of output voltage unbalance under unbalanced load conditions can be severe on the generator, other connected loads and power electronic converters, causing more losses and heating problems. To assess such adverse effects, the Voltage Unbalance Factor (VUF) for three-phase sinusoidal voltage waveforms is defined as follows [24]:

$$VUF = \frac{V^-}{V^+} \times 100\% \tag{32}$$

V^- and V^+ are the RMS voltages of the negative and positive sequence components respectively. Referring to the analysis presented in [25], these components can be calculated exactly based on only the RMS line-to-line voltages U_{ab}, U_{bc} and U_{ca} without the use of complex mathematics and the measurement of the voltage phasors. They are computed as follows:

$$V^- = \sqrt{\frac{A_m^2 - \frac{4A_s^2}{\sqrt{3}}}{2}}; \qquad V^+ = \sqrt{\frac{A_m^2 + \frac{4A_s^2}{\sqrt{3}}}{2}} \tag{33}$$

$$A_m^2 = \frac{U_{ab}^2 + U_{bc}^2 + U_{ca}^2}{3}; \quad p = \frac{U_{ab} + U_{bc} + U_{ca}}{2} \tag{34}$$

$$A_s^2 = \sqrt{p\,(p - U_{ab})\,(p - U_{bc})\,(p - U_{ca})} \tag{35}$$

The maximum permissible values of voltage unbalance should remain below 3% according to grid code requisites [26], [27].

Hereinafter, the behavior of the controller under imbalance operation is tested. The generator is first operating at normal grid conditions (balanced load). Then, unbalanced three-phase load is introduced (35% load imbalance). The response of the controlled system is illustrated in Fig.14. As foreseen, after the

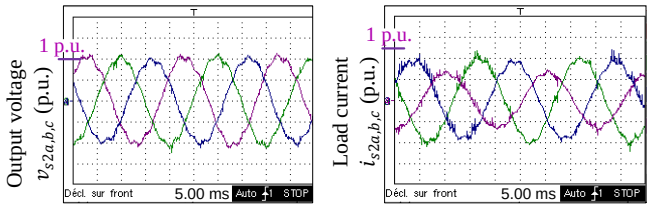

Fig. 14. Experimental results during unbalanced load conditions

connection of the unbalanced load, the stator output voltages of the CDFIG become three-phase unbalanced. However, the controller is able to effectively satisfy the requirements stated by the grid code. The obtained stator voltage unbalance factor VUF = 2.2% complies with the specified limit.

V. Conclusion

This paper presents a control scheme of the CDFIM for standalone power generation application. With its brushless structure and fractionally rated converters, this variable speed constant frequency generator is an interesting solution for many industrial applications where high level of reliability is required. Despite the complex structure of the generator, an efficient control design is elaborated with just two cascaded loops. The control target is to maintain a constant amplitude and frequency of the output voltage irrespective of load and/or speed variation.

A decoupled vector control, with indirect field orientation, is implemented for the regulation of the output stator voltage by action on the rotor current. The indirect orientation protects the frame angle from measurement noise and possible harmonic distortion on the stator voltage; particularly in weak networks with disturbances or unsymmetrical conditions. In the presented approach, simple PI controllers for each axis can be easily designed with no need to extra compensation terms or decoupling algorithm, which reduces the system cost, simplifies the digital implementation and execution time, and enhances the system robustness. Experiments are performed on the laboratory scale CDFIG. The results attest the good dynamic performances of the control system. The output voltage remains equal to its reference under a wide range of load, reference voltage and rotational speed variation.

The operation of the standalone CDFIG supplying unbalanced load is investigated too. It is proven by simulations and experiments that with up to 40% of unbalanced loads, the controller achieves to maintain a VUF within the requirements specified by the grid code. In future work, appropriate compensation methods can be considered together with the proposed controller in order to balance the stator output voltage and reject the impact of the unbalanced load. The elaborated study is under progress but preliminary results have already been presented in [28].

References

[1] N. Patin, E. Monmasson, and J.-P. Louis, "Modeling and control of a cascaded doubly fed induction generator dedicated to isolated grids," *IEEE Trans. Ind. Electron.*, vol. 56, DOI 10.1109/TIE.2009.2028358, no. 10, pp. 4207 –4219, Oct. 2009.

[2] T. D. Strous, "Brushless doubly-fed induction machines for wind turbines: developments and research challenges," *IET Elect. Power Appl.*, vol. 11, DOI 10.1049/iet-epa.2016.0118, pp. 991–1000(9), Jul. 2017.

[3] Y. Liu, W. Ai, B. Chen, and K. Chen, "Control Design of the Brushless Doubly-Fed Machines for Stand-Alone VSCF Ship Shaft Generator Systems," *J. Power Electron.*, vol. 16, DOI 10.6113/JPE.2016.16.1.259, no. 1, pp. 259–267, Jan. 2016.

[4] J. Hu, J. Zhu, and D. G. Dorrell, "A new control method of cascaded brushless doubly fed induction generators using direct power control," *IEEE Trans. Energy Convers.*, vol. 29, DOI 10.1109/TEC.2014.2325046, no. 3, pp. 771–779, Sep. 2014.

[5] A. Broadway, "Cageless induction machine," *Proc. Inst. Elect. Eng.*, vol. 118, DOI 10.1049/piee.1971.0290, no. 11, pp. 1593–1600, Nov. 1971.

[6] L. Xu, B. Guan, H. Liu, L. Gao, and K. Tsai, "Design and control of a high-efficiency doubly-fed brushless machine for wind power generator application," in *IEEE Energy Convers. Congress and Exposition ECCE, Atlanta, GA*, DOI 10.1109/ECCE.2010.5617911, pp. 2409–2416, Sep. Sept. 2010.

[7] J. Poza, E. Oyarbide, I. Sarasola, and M. Rodriguez, "Vector control design and experimental evaluation for the brushless doubly fed machine," *IET Elect. Power Appl.*, vol. 3, DOI 10.1049/iet-epa.2008.0090, no. 4, pp. 247 –256, Jul. 2009.

[8] R. Zhao, A. Zhang, Y. Ma, X. Wang, J. Yan, and Z. Ma, "The dynamic control of reactive power for the brushless doubly fed induction machine with indirect stator-quantities control scheme," *IEEE Trans. Power Electron.*, vol. 30, DOI 10.1109/TPEL.2014.2365675, no. 9, pp. 5046–5057, Sep. 2015.

Citation information: DOI 10.1109/TIE.2018.2856186, IEEE

[9] M. E. Achkar, R. Mbayed, G. Salloum, S. Leballois, N. Patin, and E. Monmasson, "New voltage sensorless approach for maximum constant power tracking of WECS based on a cascaded DFIG," in *IEEE 40th Annual Conference on Ind. Electron. Society, IECON 2014*, DOI 10.1109/IECON.2014.7048805, pp. 2185–2191, Oct. 2014.

[10] M. E. Achkar, R. Mbayed, G. Salloum, S. L. Ballois, and E. Monmasson, "Generic study of the power capability of a cascaded doubly fed induction machine," *Int. J. Elect. Power Energy Syst.*, vol. 86, DOI http://dx.doi.org/10.1016/j.ijepes.2016.09.011, pp. 61 – 70, 2017.

[11] S. Tohidi, H. Oraee, M. Zolghadri, S. Shao, and P. Tavner, "Analysis and enhancement of low-voltage ride-through capability of brushless doubly fed induction generator," *IEEE Trans. Ind. Electron.*, vol. 60, DOI 10.1109/TIE.2012.2190955, no. 3, pp. 1146–1155, Mar. 2013.

[12] S. Tohidi, P. Tavner, R. McMahon, H. Oraee, M. Zolghadri, S. Shao, and E. Abdi, "Low voltage ride-through of DFIG and brushless DFIG: similarities and differences," *Elect. Power Syst. Res.*, vol. 110, DOI http://dx.doi.org/10.1016/j.epsr.2013.12.018, pp. 64 – 72, 2014.

[13] J. Chen, W. Zhang, B. Chen, and Y. Ma, "Improved vector control of brushless doubly fed induction generator under unbalanced grid conditions for offshore wind power generation," *IEEE Trans. Energy Convers.*, vol. 31, DOI 10.1109/TEC.2015.2479859, no. 1, pp. 293–302, Mar. 2016.

[14] W. Tao, X. Wang, and L. Yongbo, "The scalar control research based on fuzzy PID of BDFM stand-alone power generation system," in *2011 International Conference on Electr. Information and Control Eng.*, DOI 10.1109/ICEICE.2011.5776928, pp. 2806–2809, Apr. 2011.

[15] X. Chen, Z. Wei, X. Gao, C. Ye, and X. Wang, "Research of voltage amplitude fluctuation and compensation for wound rotor brushless doubly-fed machine," *IEEE Trans. Energy Convers.*, vol. 30, DOI 10.1109/TEC.2015.2416515, no. 3, pp. 908–917, Sep. 2015.

[16] L. Sun, Y. Chen, J. Su, D. Zhang, L. Peng, and Y. Kang, "Decoupling network design for inner current loops of stand-alone brushless doubly fed induction generation power system," *IEEE Trans. Power Electron.*, vol. 33, DOI 10.1109/TPEL.2017.2734108, no. 2, pp. 957–963, Feb. 2018.

[17] M. Adamowicz, R. Strzelecki, and D. Wojciechowski, "Steady state analysis of twin stator cascaded doubly fed induction generator," in *Compatibility in Power Electron, CPE '07*, DOI 10.1109/CPE.2007.4296534, pp. 1–5, May. 2007.

[18] C. Cook and B. Smith, "Stability and stabilisation of doubly-fed single-frame cascade induction machines," *Proc. Inst. Electr. Eng.*, vol. 126, DOI 10.1049/piee.1979.0199, no. 11, pp. 1168 –1174, Nov. 1979.

[19] R. McMahon, P. Roberts, X. Wang, and P. Tavner, "Performance of BDFM as generator and motor," *IEE Proc. Elect. Power Appl.*, vol. 153, DOI 10.1049/ip-epa:20050289, no. 2, pp. 289–299, Mar. 2006.

[20] G. Esfandiari, M. Ebrahimi, A. Tabesh, and M. Esmaeilzadeh, "Dynamic modeling and analysis of cascaded DFIMs in an arbitrary reference frame," *IEEE Trans. Energy Convers.*, vol. 30, DOI 10.1109/TEC.2015.2416273, no. 3, pp. 999–1007, Sep. 2015.

[21] M. E. Achkar, R. Mbayed, G. Salloum, N. Patin, S. L. Ballois, and E. Monmasson, "Power operating domain of a cascaded doubly fed induction machine," *Math. Comput. Simul.*, DOI http://dx.doi.org/10.1016/j.matcom.2015.02.002, InPress, 2015.

[22] J. Maciejowski, *Multivariable Feedback Design*. Electronic systems engineering series. Addison-Wesley, 1989.

[23] V.-T. Phan, T. Logenthiran, W. Woo, D. Atkinson, and V. Pickert, "Analysis and compensation of voltage unbalance of a DFIG using predictive rotor current control," *Int. J. Elect. Power Energy Syst.*, vol. 75, DOI http://dx.doi.org/10.1016/j.ijepes.2015.08.020, pp. 8 – 18, 2016.

[24] V.-T. Phan and H.-H. Lee, "Improved predictive current control for unbalanced stand-alone doubly-fed induction generator-based wind power systems," *Electric Power Applications, IET*, vol. 5, DOI 10.1049/iet-epa.2010.0107, no. 3, pp. 275–287, Mar. 2011.

[25] J. Ghijselen and A. Van den Bossche, "Exact voltage unbalance assessment without phase measurements," *IEEE Trans. Power Syst.*, vol. 20, DOI 10.1109/TPWRS.2004.841145, no. 1, pp. 519–520, Feb. 2005.

[26] *Grid Code 2015 for Small Scale Distributed Generation (SSDG) Net Metering Scheme*, Version 2.2 - June 2017.

[27] F. Ghassemi and M. Perry, *Review of Voltage Unbalance Limit in The GB Grid Code CC.6.1.5 (b)*, October 2014.

[28] M. E. Achkar, R. Mbayed, G. Salloum, S. L. Ballois, and E. Monmasson, "Compensation of voltage unbalance of a standalone cdfig using repetitive rotor current control," in *19th European Conference on Power Electron. and Applications (EPE'17 ECCE Europe)*, DOI 10.23919/EPE17ECCEEurope.2017.8099020, pp. P.1–P.9, Sep. 2017.

M. EL Achkar received the Electrical Ing.Dipl. from the Lebanese University, Lebanon, in 2012, the M.Sc. degree in Industrial Control from the Université de Technologies de Compiègne (UTC), France in 2012 and the PhD degree in Electrical Engineering from Cergy-Pontoise University, France in 2016. Her research interests include modeling analysis and control of electrical machines, power converters and renewable energy.

R. Mbayed has received an Electrical Engineering diploma from the Lebanese University, Lebanon, in 2006, a M.Sc. degree in Industrial Control from the Université de Technologies de Compiègne (UTC), France in 2007 and a PhD in Electrical Engineering from Cergy-Pontoise University, France in 2012. She is currently an Associate Professor at the Lebanese University. Her research interests concern modeling and control of non-conventional electrical machines and management of renewable energy sources.

G. Salloum has received the diploma in Electromechanical Engineering from the Ecole Supérieure d'Ingénieurs of Beirut (ESIB), Lebanon in 1988, and the Ph.D. degree in Electrical Engineering from the Institut National Polytechnique (INP), Toulouse, FRANCE in 2007. He is currently a Professor and the head of CERGE research team at the Lebanese University. He is a senior member of the IEEE. His research interests concern modeling and control of non-conventional electrical machines, power converters and the management of renewable energy sources.

N. Patin (S'06-M'07-SM'12) was born in Châteauroux, France, in 1979. He received the M.Sc. and Ph.D. degrees from the Ecole Normale Supérieure de Cachan, France, in 2004 and 2006, respectively. Since September 2007, he has been an Associate Professor at the Electromechanics Laboratory, University of Technology of Compiègne, France. His current research interests include control strategies of power converters, aging of DC capacitors and electromagnetic compatibility, especially in embedded applications.

E. Monmasson (M'96-SM'06) received the Ing. and Ph.D. degrees from the Ecole Nationale Superieure d'Ingénieurs d'Electrotechnique d'Electronique d'Informatique et d'Hydraulique de Toulouse, France, in 1989 and 1993, respectively. Since 2003, he is a Full Professor at the University of Cergy-Pontoise, France. He is also with SATIE laboratory, UMR CNRS 8029, Cergy-Pontoise. He is the author or coauthor of 3 books and more than 200 scientific papers. His current research interests include the control of power electronics, electrical motors and generators, and FPGA-based and SoC-based industrial control systems. Dr. Monmasson was the Chair of the technical committee on Electronic Systems-on-Chip of the IEEE Industrial Electronics Society (2008-2011). He is also a member of the steering committee of the European Power Electronics Association and he was the Chair of the technical committee of the International Association for Mathematics and Computers in Simulation (2011-2017). He is an Associate Editor of the IEEE-TIE and the IEEE-TII.